Available online at www.sciencedirect.com
ScienceDirect
Trans. Nonferrous Met. Soc. China 31(2021) 2232−2249
Transactions of Nonferrous Metals Society of China
www.tnmsc.cn

Microstructure and high temperature tensile properties of Al−Si−Cu−Mn−Fe alloys prepared by semi-solid thixoforming

Bo LIN[1], Tao FAN[1], Hao-yu LI[1], Yu-liang ZHAO[2], Wei-wen ZHANG[3], Kun LIU[4]

1. School of Mechanical Engineering, Guizhou University, Guiyang 550025, China;
2. School of Mechanical Engineering, Dongguan University of Technology, Dongguan 523808, China;
3. School of Mechanical and Automotive Engineering,
South China University of Technology, Guangzhou 510640, China;
4. Department of Applied Science, University of Quebec at Chicoutimi, Quebec, Canada

Received 22 August 2020; accepted 14 May 2021

Abstract: The differences in the microstructure and elevated temperature tensile properties of gravity die cast, squeeze cast, and semi-solid thixoformed Al−Si−Cu−Mn−Fe alloys after thermal exposure at 300 °C were discussed. The results demonstrate that the elevated temperature tensile properties of semi-solid thixoformed alloys were significantly higher than those of gravity die cast and squeeze cast alloys, especially after thermal exposure for 100 h. The ultimate tensile strength (UTS) of semi-solid thixoformed alloys after thermal exposure at 300 °C for 0.5, 10 and 100 h were 181, 122 and 110 MPa, respectively. The UTS values of semi-solid thixoformed alloys were higher than those of heat resistant aluminum alloys used in commercial applications. The enhanced elevated temperature tensile properties of semi-solid thixoformed experimental alloys after thermal exposure can be attributed to the combined reinforcement of precipitation strengthening and grain boundary strengthening due to thermally stable intermetallic phases as well as suitable grain size.

Key words: Al−Si alloys; iron-rich intermetallics; semi-solid thixoforming; microstructure; tensile properties; thermal exposure

1 Introduction

Al−Si cast alloys have excellent cast ability and high specific strength, corrosion resistance, and thermal conductivity. Therefore, the Al−Si alloys have a broad range of applications as heat-resistant, light, structural components in the aerospace, military, marine, and transportation industries. To develop green economy, it is crucial to improve the engine efficiency of diesel oil engines to save energy and reduce emission. Consequently, the heat-resistant Al−Si alloys with super high performance in diesel oil engine components have drawn significant attention in the aerospace, military, marine, and transportation industries.

Thermal exposure testing at elevated temperatures has been commonly employed to simulate the temperature changes and stress states of the automotive engines under real service conditions. Also, it is used as a basis for the automotive engine design. Elevated temperature thermal exposure may cause some changes in the microstructure, such as the coarsening of secondary intermetallic particles, increase in precipitate free zones, dislocation movement, and grain boundary sliding [1]. Therefore, the tensile properties are affected by the evolution of microstructure after thermal exposure treatment. The addition of elements to form heat-resistant phases, such as Sc

Corresponding author: Bo LIN, E-mail: linbo1234@126.com; Yu-liang ZHAO, E-mail: zhaoyl@dgut.edu.cn
DOI: 10.1016/S1003-6326(21)65651-0

by DING et al [2], Zr by TZENG et al [3], Ni and Mn by ABDELAZIZ et al [4], and Mn and Fe by WANG et al [5], is an efficient approach to improve the elevated temperature tensile properties of heat-resistant Al−Si alloys after thermal exposure. DING et al [2] reported that the formation of nano Al_3Sc precipitates can be responsible for the improvement of tensile properties of A356 alloys under thermal exposure at 200 °C. TZENG et al [3] found that the Zr addition improved the elevated temperature tensile properties of A357 alloys after thermal exposure at 250 °C, which can be attributed to the formation of Al_3Zr precipitates. ABDELAZIZ et al [4] concluded that the addition of Mn or Ni contributed only little to tensile properties of Zr-containing Al−Si−Cu−Mg cast alloys after elevated temperature thermal exposure. In our previous work [6], gravity die cast alloys with different Ti and Cu additions were designed and excellent elevated temperature tensile properties after thermal exposure at 300 °C were achieved. These improved tensile properties could be attributed to high thermal stability of precipitated particles, such as T ($Al_{20}Cu_2Mn_3$) and α-Fe ($Al_{15}(FeMn)_3(CuSi)_2$) phases. However, the improvement rate in elevated temperature tensile properties with grain refinement decreased with the rise in thermal exposure duration. The reason for the phenomenon can be attributed to the grain boundary sliding during long thermal exposure duration [6]. Hence, to develop the heat-resistant Al alloys with highly enhanced elevated temperature tensile properties after long thermal exposure, it is important to increase the precipitated particles in the aluminum matrix and the heat-resistant intermetallics around the grain boundary, as well as control the grain size.

Semi-solid thixoforming is a green casting technology, which was firstly developed by FLEMINGS et al [7]. Semi-solid thixoforming increases the number of precipitated particles in the α(Al) matrix because of high cooling rate during high-pressure solidification. Also, the heat-resistant intermetallics precipitate around the grain boundary during semi-solid thixoforming [8]. As reported by ZHANG et al [9], the grain size can be controlled by adjusting the holding time during semi-solid isothermal treatment process. Therefore, semi-solid thixoforming may be an efficient method to develop heat-resistant aluminum alloys. Till date, most studies have focused on the room temperature tensile properties of semi-solid alloys [10−13]. KANG and SOHN [10] found that Si content and forging pressure are important for improving the mechanical properties of semi-solid Al−Si−Mg alloys at room temperature. QI et al [11] reported that the thermal conductivity, corrosion resistance, and room temperature mechanical properties were improved by using rheological high pressure die casting. KUMAR et al [12,13] studied the effect of semi-solid thixoforming on the tensile properties of A356 and A356−5TiB_2 alloys and found that the improved room temperature mechanical properties of semi-solid thixoformed alloys were achieved. Only a few researchers have reported on the elevated temperature tensile properties of semi-solid alloys after thermal exposure.

Herein, semi-solid thixoforming was employed to develop experimental alloys with high-performance tensile properties under elevated temperature thermal exposure. The differences in the microstructures and elevated temperature tensile properties of gravity die cast, squeeze cast, and semi-solid thixoformed alloys have been discussed in detail. This study is beneficial to widening the industrial applications of semi-solid aluminum alloys in the fabrication of light, heat-resistant, structural components in the aerospace, military, marine, and transportation industries. The Fe content is considered to be unavoidable in aluminum alloys and always is accumulated after recycling. The development of Al−Si−Cu−Mn alloys with high Fe content would be beneficial to the recycling of waste aluminum alloys.

2 Experimental

The experimental alloys were prepared by pure Al (99.5 wt.%) and Al−20wt.%Si, Al−50wt.%Cu, Al−5wt.%Mg, Al−10wt.%Mn, Al−5wt.%Fe, and Al−5wt.%Ti master alloys. The chemical composition of the experimental alloys is listed in Table 1.

Table 1 Chemical composition of experimental alloy (wt.%)

Si	Cu	Mn	Fe	Ti	Mg	Sr	Al
6.72	3.90	0.59	0.59	0.22	0.12	0.01	Bal.

The detailed melting and degassing processes of the experimental alloys have been presented in our earlier-stage work [6]. The aluminum melts were poured into an H13 cylindrical die and solidified at 0 MPa to obtain the gravity die cast samples. For the squeeze cast samples, the aluminum melts were poured into an H13 cylindrical die and solidified at 75 MPa. The pouring and die temperatures were 730 and 250 °C, respectively. Our experimental alloys are similar to the A319 alloys. The appropriate process temperature for semi-solid isothermal heat treatment of A319 alloys is about 571 °C [14,15]. The semi-solid isothermal treatment samples with the size of *d*10 mm × 10 mm were cut from the gravity die cast samples. Then, the samples were isothermally treated in a holding furnace at 550−580 °C for 30−90 min. Then, the semi-solid isothermal treatment samples were immediately quenched in room temperature water to maintain the semi-solid microstructure. The optimization of semi-solid isothermal treatment process was determined by the suitable liquid fraction and granule roundness of α(Al) for semi-solid thixoforming. Finally, the semi-solid samples were formed in an H13 cylindrical die under 75 MPa.

The shape factor of α(Al) and the liquid fraction were quantitatively calculated by using Image-Pro Plus software. The shape factor of α(Al) can be described using Eq. (1):

$$K = \frac{4\pi A}{P^2} \tag{1}$$

where K is the shape factor of α(Al), A is the surface area, and P is the perimeter.

According to the reports by WANG et al [5], the T6 heat treatment is generally employed for Al−Si alloys to stabilize the microstructure. The T6 heat treatment process can also be found in our previous work [6]. After T6 heat treatment, the samples were machined into standard tensile test bars of 70 mm in length and 5 mm in diameter. Then, the tensile specimens were placed in a heat treatment furnace at the temperature of 300 °C for different time (0.5, 10, and 100 h). The elevated temperature tensile properties were also studied in our previous work [16]. The tensile property values were the average of at least three testing samples.

The samples for microstructural observation came from the gripping parts of the tensile properties test bars. To reveal the intermetallics and precipitated particles, the samples were etched in a Keller solution for 10−15 s. Subsequently, a Leica optical metallographic microscope was employed to observe the microstructure of the samples. The samples for grain structure observation were etched in a 5 vol.% HBF_4 solution under a direct current source at the voltage of 10 V and current of 0.1 A for 1.5 min. Then, the samples were etched in the solution of Keller reagent. The grain size of the alloys was quantitatively analyzed by using the linear intercept method with a Leica optical microscope equipped with the image analysis software. The morphologies of secondary inter-metallic phases and surface fractures were analyzed under a scanning electron microscope (Nova Nano SEM 430). The changes in the precipitates and dislocation in the α(Al) matrix were analyzed using a transmission electron microscope (JEOL JEM−3010) at 200 kV.

3 Results

3.1 Optimization of semi-solid isothermal treatment process

Figure 1 displays the microstructures of the alloys after semi-solid isothermal treatment at different temperatures for 90 min. When the semi-solid isothermal treatment temperature was 550 °C, the microstructure demonstrated no clear change. With the increase in semi-solid isothermal treatment temperature, the liquid fraction clearly increased, and the grains became globular. When the semi-solid isothermal treatment temperature was 580 °C, the liquid fraction slightly increased, and the grains became more globular. The shape factor of α(Al) was 0.65.

Figure 2 shows the microstructures of the alloys after semi-solid isothermal treatment at 580 °C for different time. When the semi-solid isothermal treatment time was 30 min, a little liquid was found on the samples. With the rise in semi-solid isothermal treatment time, the liquid fraction clearly increased, and the grains became globular. With further increase in semi-solid isothermal treatment time to 90 min, that is, 120 min, grains became more globular. However, when the semi-solid isothermal treatment time was above 90 min, the liquid faction tended to reach equilibrium.

As per the results, the α(Al) displayed spheroidizing during the semi-solid isothermal heat treatment. The mechanism of spheroidizing has been discussed in several works [17−20]. The mechanism of spheroidizing can be attributed to the evolution of α(Al) dendrite edge blunting, α(Al)

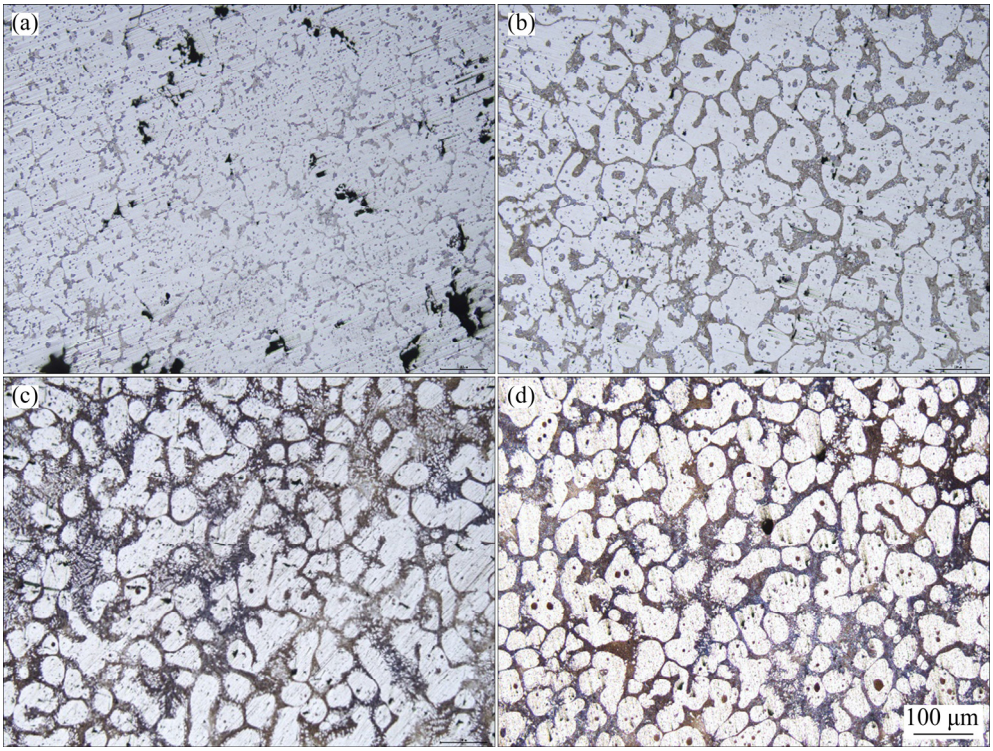

Fig. 1 Microstructures of alloys after semi-solid isothermal treatment at different temperatures for 90 min: (a) 550 °C; (b) 560 °C; (c) 570 °C; (d) 580 °C

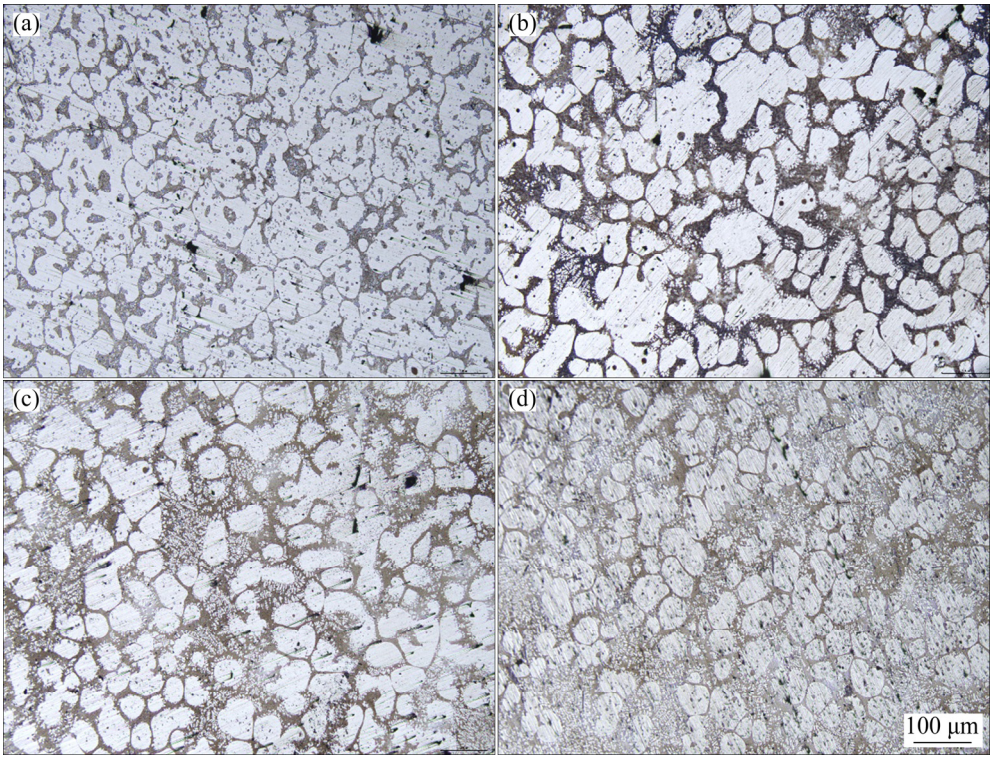

Fig. 2 Microstructures of alloys after semi-solid isothermal treatment at 580 °C for different time: (a) 30 min; (b) 60 min; (c) 90 min; (d) 120 min

dendrite dissolution, grain spheroidization, grain maturation, and coarsening [17,18]. Figure 3 displays the liquid fractions of semi-solid isothermal treatment samples at different temperatures and time. It can be found that the liquid fraction increased with rise in temperature and time. When the semi-solid isothermal treatment temperature was 580 °C and time was 90 min, the liquid fraction of the samples was about 40%. Most of the works have reported that the suitable liquid fraction for semi-solid thixoforming is 30−50% [19,20]. Hence, the appropriate process for semi-solid isothermal heat treatment of 4Cu−0.2Ti alloys is heating at 580 °C for 90 min.

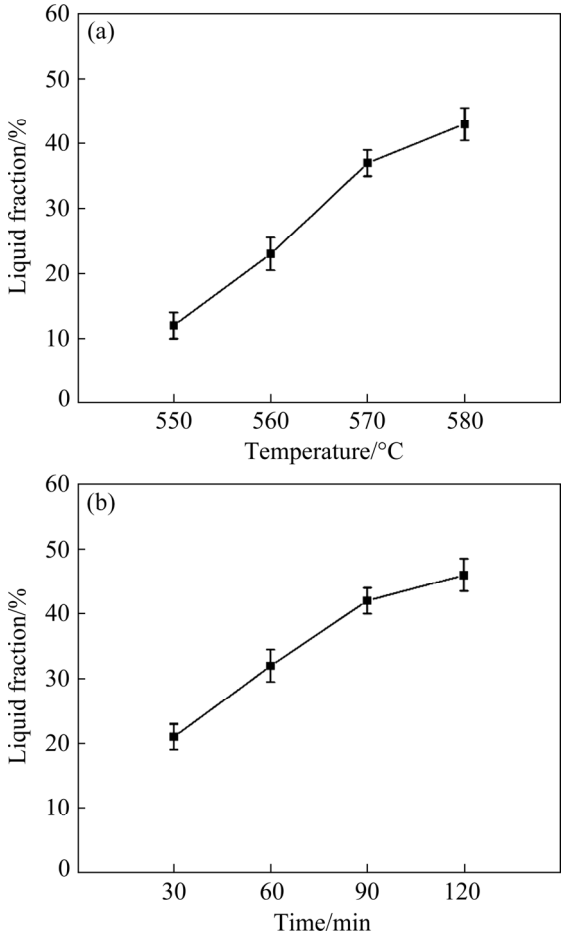

Fig. 3 Liquid fractions of semi-solid isothermal treatment samples at different temperatures (a) and time (b)

3.2 Secondary intermetallics in experimental alloys

Figure 4 shows the OM, SEM image and energy dispersive X-ray spectroscopy (EDS) maps of the gravity die cast experimental alloys. The secondary intermetallics included Al_2Cu, α-Fe ($Al_{15}(FeMn)_3(CuSi)_2$), Si particles, β-Fe(Al_7Cu_2Fe), and TiAlSi phases, which have also been reported in our previous work [6].

Figure 5 presents the microstructures of experimental alloys formed by different processes after thermal exposure for 0.5 h. Several pores and needle-like phases were found in the gravity die cast samples. In the squeeze cast and semi-solid thixoformed samples, the porosities were significantly decreased as compared to the gravity die cast samples. Also, the needle-like intermetallic phases in the squeeze cast and semi-solid thixoformed samples disappeared, which indicated that the applied pressure efficiently prevented the formation of needle-like intermetallic phase. However, some large block-shaped iron-rich intermetallics, called sludge, were found in the squeeze cast samples.

The sludge consists of the primary iron-rich intermetallics, which is formed in the Al−Si−Cu alloys depending on the Fe, Mn, and Cr contents, the holding temperature, as well as the cooling rate. The formation tendency of sludge in the Al−Si−Cu alloys can be predicted by the sludge factor equation. The sludge factor is affected by the Fe, Mn, and Cr contents, and can be described by Eq. (2):

$$s_f=w_{Fe}+2w_{Mn}+3w_{Cr} \quad (2)$$

where s_f is the sludge factor; w_{Fe}, w_{Mn}, and w_{Cr} are the mass fractions of Fe, Mn, and Cr, respectively. Herein, the sludge factor was 1.77 (Mn, 0.59 wt.%; Fe, 0.59 wt.%). HWANG et al [21] reported that when the sludge factor was 1.8 (Mn, 0.65 wt.%; Fe, 0.5 wt.%), there was no sludge formed in the A319 alloys. However, when the sludge factor was 2.2 (Mn, 0.85 wt.%; Fe, 0.5 wt.%), the sludge was formed in the A319 alloys.

The holding temperature of sludge formation depends on the Fe content, which can be described as follows:

$$T_{sp}=645.7+34.2w_{Fe}^2 \quad (3)$$

where T_{sp} is the sludge precipitation temperature. As per SHABESTARI [22], when the holding temperature was below the sludge precipitation temperature (657.6 °C in this study), the sludge was formed in the Al−Si−Cu alloys. The holding temperature in this study was 730 °C; hence, the sludge was not formed in the gravity die cast

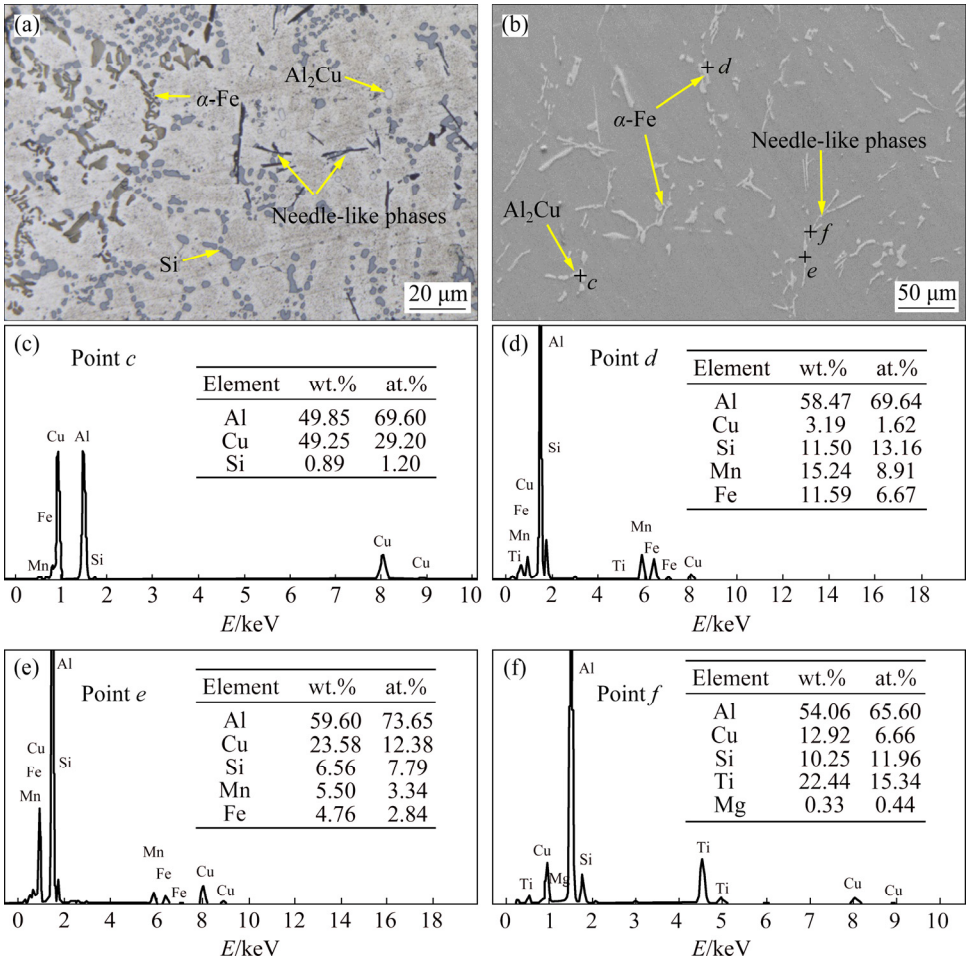

Fig. 4 Images of microstructures (a, b) and EDS maps (c−f) of gravity die cast experimental alloys: (a) OM image; (b) SEM image; (c) Al_2Cu; (d) α-Fe; (e) β-Fe; (f) TiAlSi

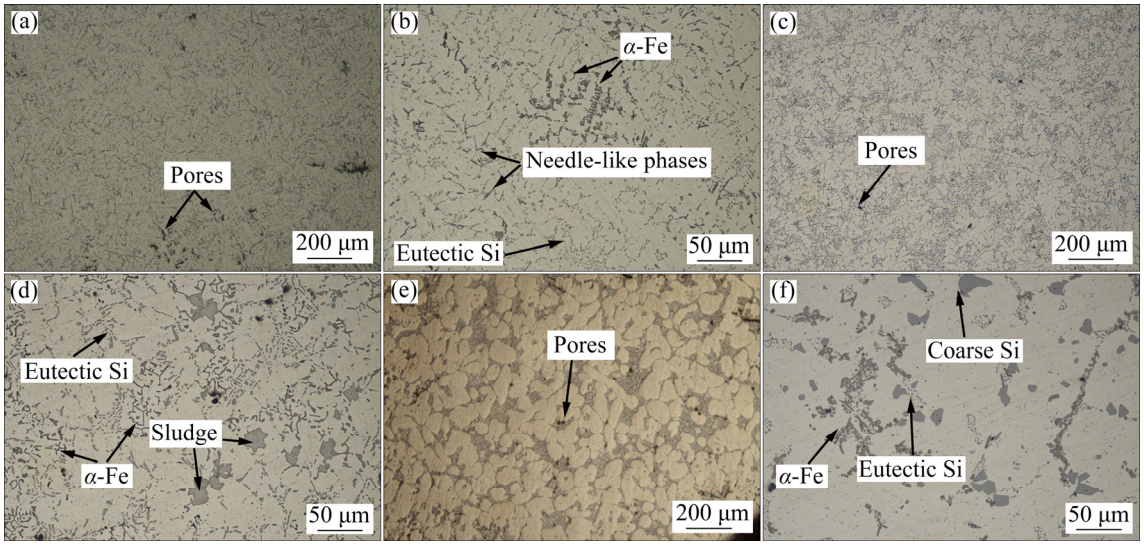

Fig. 5 Microstructures of experimental alloys formed by different processes after thermal exposure for 0.5 h: (a, b) Gravity die cast alloys; (c, d) Squeeze cast alloys; (e, f) Semi-solid thixoformed alloys

samples. The formation of sludge in squeeze cast samples can be attributed to the high cooling rate. HE also suggested that the high cooling rate promotes the formation of sludge, which can be attributed to the segregation of iron at high cooling rate in the squeeze cast samples.

Moreover, some coarse block-shaped Si particles were found in the semi-solid thixoformed samples, which can be attributed to the growth of Si particles during the semi-solid isothermal treatment. Besides, Fe-rich intermetallics and Si developed chain- or annular-like distributions around the grain boundary.

Figure 6 displays the microstructures of experimental alloys formed by different processes after thermal exposure for 100 h. Nearly no microstructural changes were found in the samples, indicating that the secondary intermetallics, such as Si and Fe-rich intermetallics, remained stable after thermal exposure for 100 h.

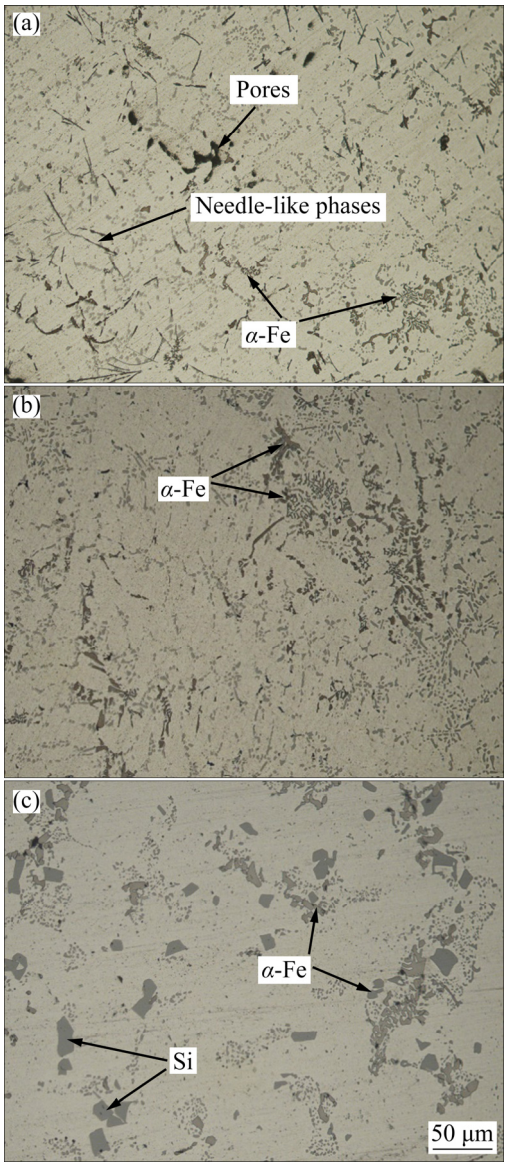

Fig. 6 Microstructures of experimental alloys formed by different processes after thermal exposure for 100 h: (a) Gravity die cast alloys; (b) Squeeze cast alloys; (c) Semi-solid thixoformed alloys

Figure 7 illustrates the grain sizes of experimental alloys formed by different processes after thermal exposure for 0.5 h. The grain size was significantly refined in the squeeze cast samples. The grain sizes of the alloys formed by different processes were quantitatively analyzed. The grain size of the squeeze cast alloy was estimated to be 118 μm, which was significantly less than that of the gravity die cast alloy (437 μm). While, that for semi-solid thixoformed alloy was estimated to be 209 μm, which was much coarsened than that of the squeeze cast alloy. The coarsening of grain size in semi-solid thixoformed alloys can be attributed to the grain growth during the semi-solid isothermal treatment.

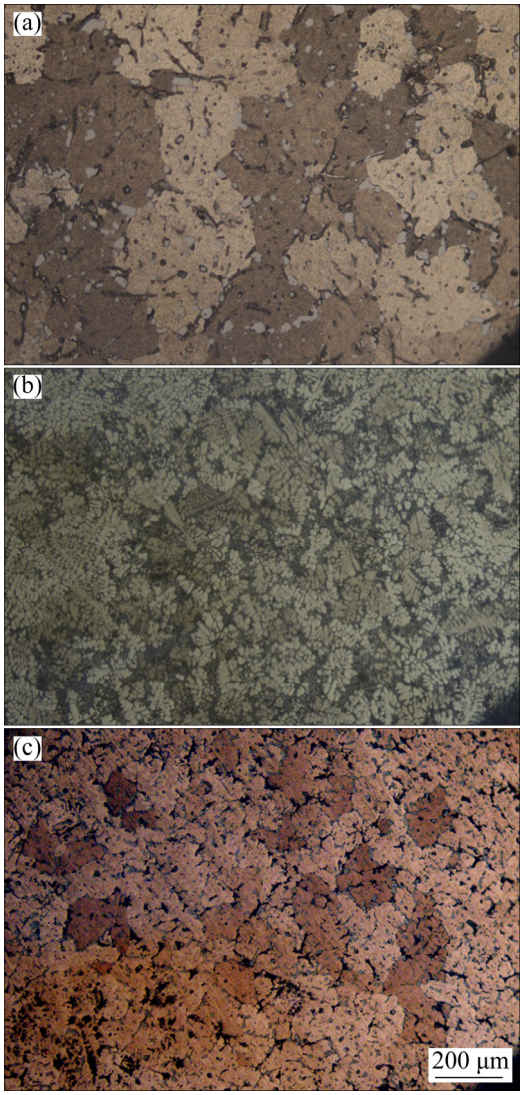

Fig. 7 Grain sizes of experimental alloys formed by different processes after thermal exposure for 0.5 h: (a) Gravity die cast alloys; (b) Squeeze cast alloys; (c) Semi-solid thixoformed alloys

3.3 Precipitated particles in *α*(Al) matrix

Figure 8 shows changes in the number of precipitated particles in the *α*(Al) matrix of alloys formed by different processes after elevated temperature thermal exposure for different time. The OM images suggested that the precipitated particles were significantly decreased with the increase in thermal exposure time. Furthermore, the precipitated particles in the squeeze cast and semi-solid thixoformed alloys increased significantly compared to the gravity die cast alloys, which can be attributed to the increase in solid solubility because of the applied pressure.

Figure 9 shows the TEM images of the precipitated particles of squeeze cast experimental alloy after thermal exposure at 300 °C for 0.5 h. Figure 9(a) displays the high-resolution TEM image of the $\theta'(Al_2Cu)$ phase. Some rod- and block-shaped phases were also observed in the experimental alloy (Fig. 9(b)). The EDS results in Fig. 9(c) demonstrate that the alloy contains Al, Cu, and Mn elements, indicating that the rod-shaped phase was T ($Al_{20}Cu_2Mn_3$). The EDS results in Fig. 9(d) show that the alloy contains Al, Cu, Mn, Fe, and Si elements, which suggests that the block-shaped phase is the α-$Fe(Al_{15}(FeMn)_3(CuSi)_2)$ phase. Consequently, the dispersoids in the experimental alloys were nano-sized $\theta'(Al_2Cu)$ and α-Fe and micro-sized $T(Al_{20}Cu_2Mn_3)$, which was reported in our previous work [6] and other reports [23,24]. As the change in $\theta'(Al_2Cu)$ has been studied before and after thermal exposure at 300 °C, the evolution of $\theta'(Al_2Cu)$ was not studied in this work [25].

TEM observations were employed to study the morphological changes in the dispersoids in Al matrix. Figure 10 shows the TEM images of the experimental alloys formed by different processes for different thermal exposure time. When the

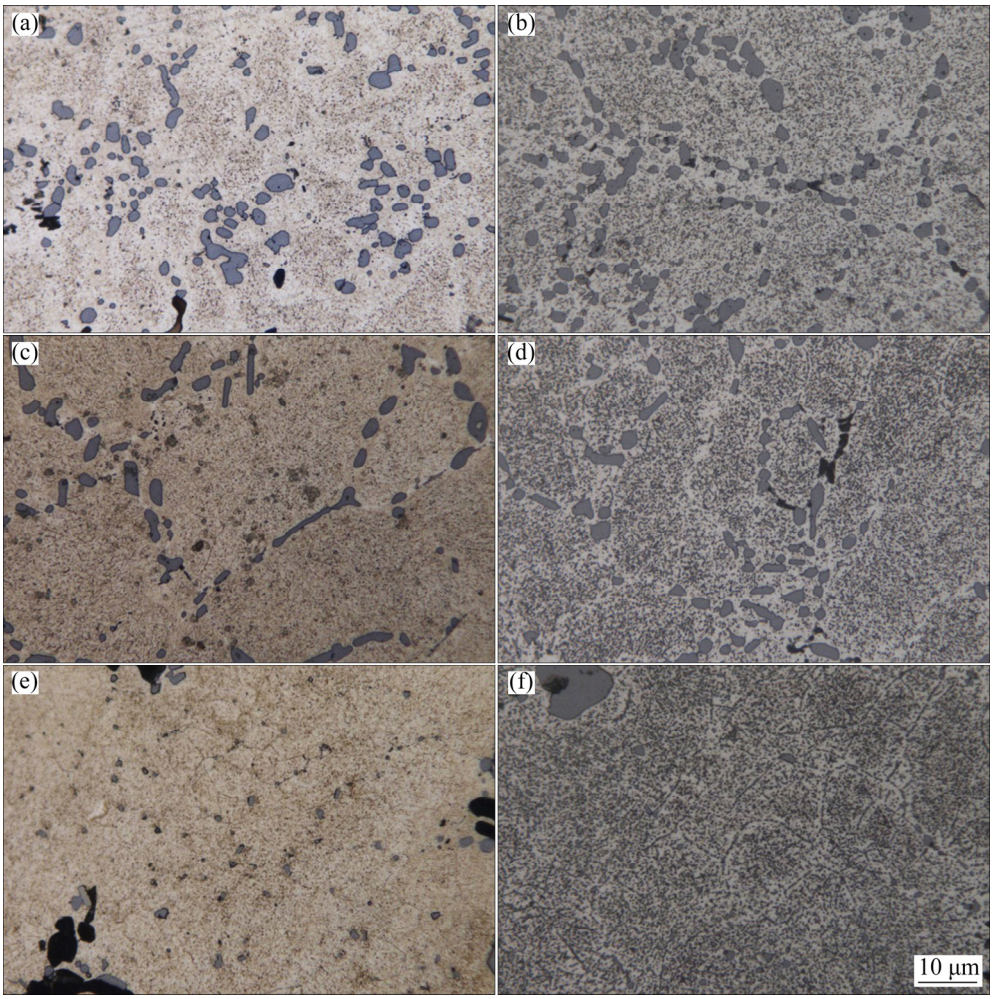

Fig. 8 Morphologies of precipitates in *α*(Al) matrix observed under OM: (a) Gravity die cast alloys, 0.5 h; (b) Gravity die cast alloys, 100 h; (c) Squeeze cast alloys, 0.5 h; (d) Squeeze cast alloys, 100 h; (e) Semi-solid thixoformed alloys, 0.5 h; (f) Semi-solid thixoformed alloys, 100 h

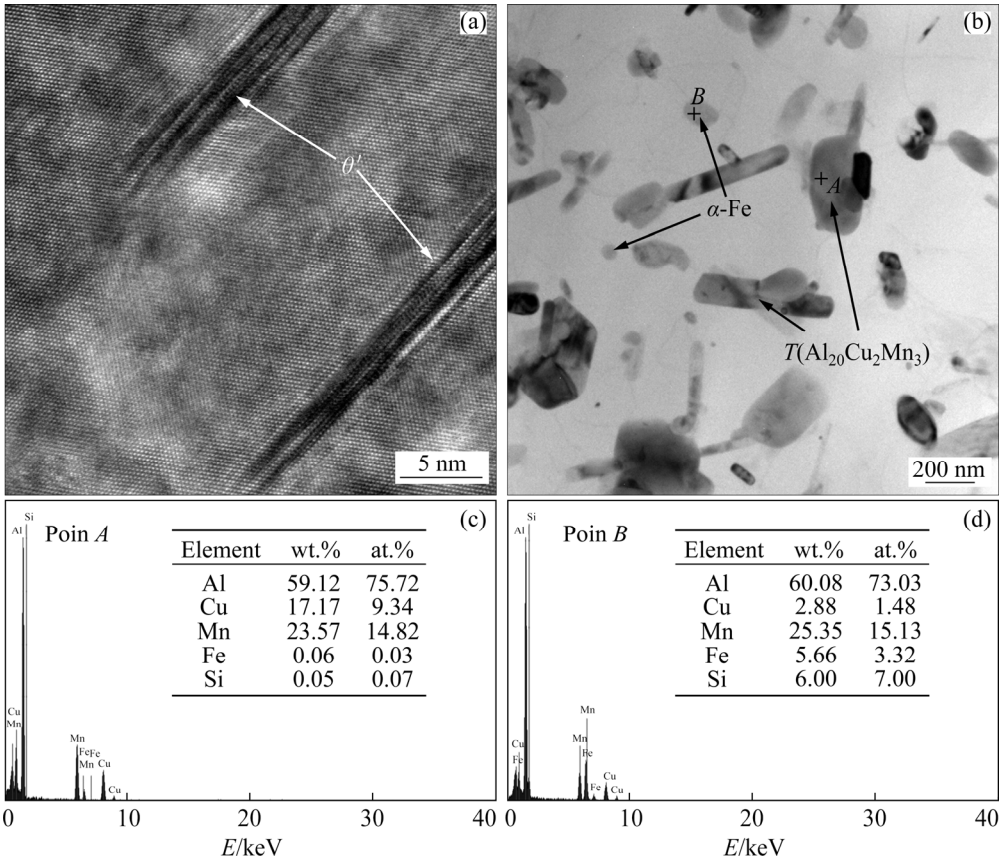

Fig. 9 Dispersoid morphologies (a, b) and EDS spectra (c, d) of squeeze cast experimental alloys after thermal exposure at 300 °C for 0.5 h: (a) TEM image of $\theta'(Al_2Cu)$; (b) TEM image of $T(Al_{20}Cu_2Mn_3)$ and α-Fe; (c) EDS spectrum of $T(Al_{20}Cu_2Mn_3)$; (d) EDS spectrum of α-Fe

thermal exposure time was 0.5 h, several nano-sized $\theta'(Al_2Cu)$ phases were observed in the samples. When the thermal exposure time was further increased to 100 h, the $\theta'(Al_2Cu)$ decreased significantly. In the squeeze cast and semi-solid thixoformed samples, the size of dispersoids was significantly decreased, while their volume fraction was significantly increased as compared to that of the gravity die cast samples.

The size of dispersoids was quantitatively analyzed using the Image J software (Fig. 11). The size of $\theta'(Al_2Cu)$ was measured for the samples after thermal exposure for 0.5 h. The sizes of $T(Al_{20}Cu_2Mn_3)$ and α-Fe phases were measured for the samples after thermal exposure for 100 h. The size of $\theta'(Al_2Cu)$ was measured to be 136 nm in gravity die cast samples, 58 nm in squeeze cast samples, and 62 nm in semi-solid thixoformed samples. The size of α-Fe was measured to be 138 nm in gravity die cast samples, 64 nm in squeeze cast samples, and 68 nm in semi-solid thixoformed samples. Finally, the size of $T(Al_{20}Cu_2Mn_3)$ was measured to be about 1 μm and little changes were observed among different forming processes.

3.4 Elevated temperature tensile properties of experimental alloys after thermal exposure

Figure 12 demonstrates elevated temperature tensile properties of alloys after thermal exposure. The increase of thermal exposure duration deteriorated the elevated temperature strength but increased the elongation. As the thermal exposure time increased from 0.5 to 10 h, the thermal exposure strength decreased sharply, and then, it reduced a little as the thermal exposure time was further increased to 100 h. The elevated temperature tensile properties of the squeeze cast alloys demonstrated higher values than the gravity die cast alloys after thermal exposure for 0.5 h, which were then decreased to almost the same values after thermal exposure for 100 h. The elevated temperature tensile properties of the semi-solid thixoformed alloys displayed significantly higher

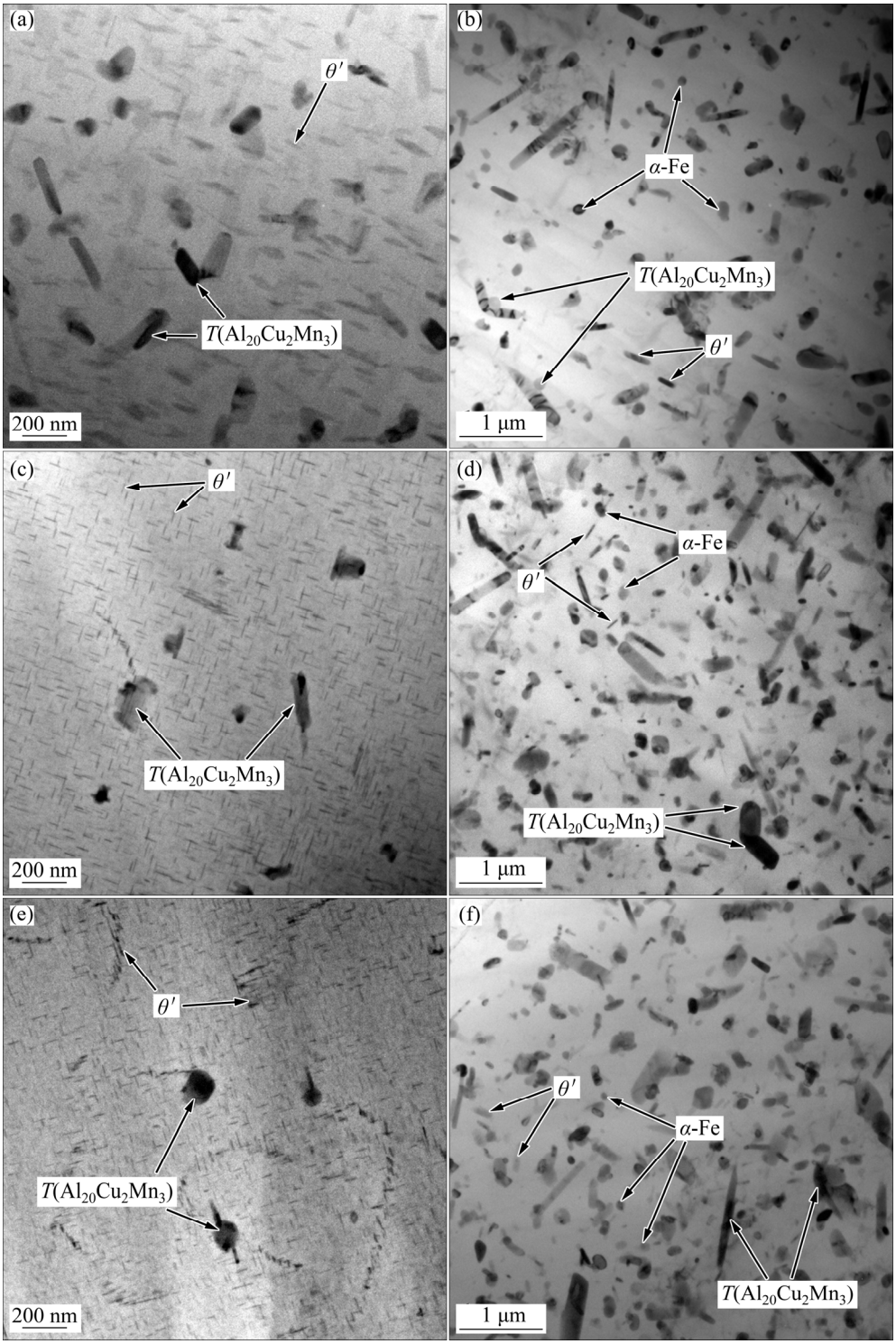

Fig. 10 Dispersoid morphologies in α(Al) matrix of alloys observed under TEM: (a) Gravity die cast alloys, 0.5 h; (b) Gravity die cast alloys, 100 h; (c) Squeeze cast alloys, 0.5 h; (d) Squeeze cast alloys, 100 h; (e) Semi-solid thixoformed alloys, 0.5 h; (f) Semi-solid thixoformed alloys, 100 h

values than the gravity die cast and squeeze cast alloys, especially, after thermal exposure for 100 h. KAUFMAN [26] investigated the UTS of commercial aluminum alloys after thermal exposure at 300 °C for different time. WANG et al [5] studied the high temperature strength of experimental alloys and found that the UTS reached up to 144 MPa after thermal exposure at 300 °C for 0.5 h. LIAN et al [27] and SUI et al [28] also reported the UTS of Al−12Si−4Cu−2Ni−0.8Mg to

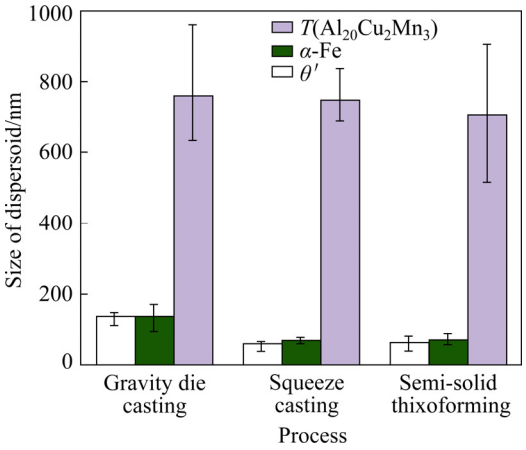

Fig. 11 Dispersoid size in alloys formed via different processes

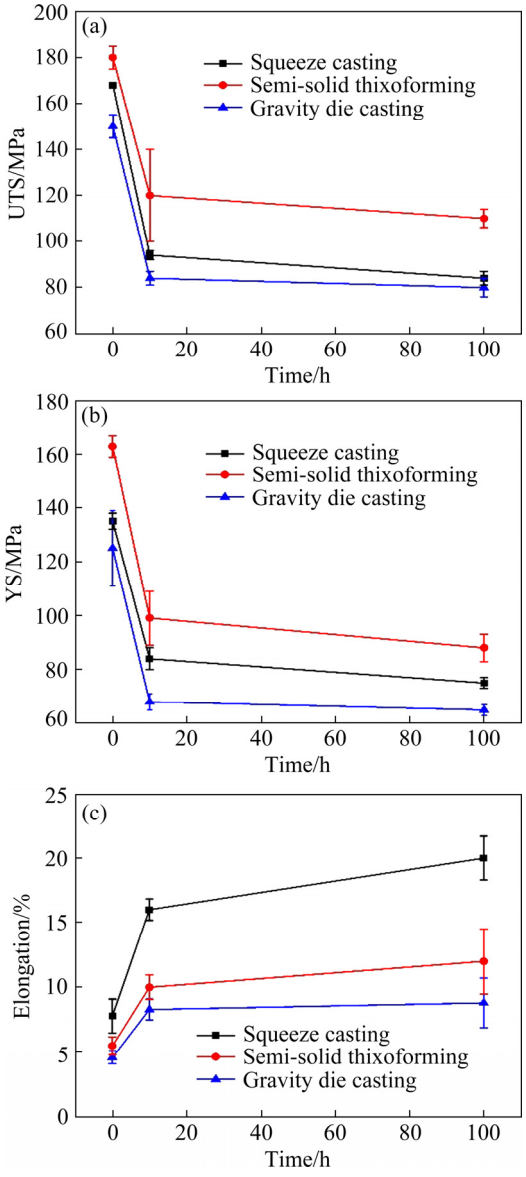

Fig. 12 Elevated temperature tensile properties of alloys formed via different processes after thermal exposure: (a) UTS; (b) YS; (c) Elongation

be 109.5 and 140 MPa, respectively. AIKAWA et al [29] developed two kinds of Al−Si−Cu−Mg−Ni−V piston alloys with different Cu contents and found that Cu content had no clear effect on the elevated temperature UTS of the alloy. TAKASAKI and YOSHIMURA [30] prepared Al−13.0Si−3.3Cu−1.3Mg−1.6Zn piston alloys and found that the elevated temperature UTS of this piston alloy was 132−145 MPa. Herein, to evaluate the elevated temperature UTS, the results of the experimental alloys formed by gravity die cast, squeeze cast, and semi-solid thixoforming processes were compared to those of the heat-resistant aluminum alloys for commercial applications in the above references after thermal exposure at 300 °C. The results are presented in Table 2. The elevated temperature UTS values of all the experimental alloys were higher than those of the heat-resistant aluminum alloys for commercial applications, such as the wrought aluminum alloy and Al−Si alloys. For instance, after thermal exposure at 300 °C for 0.5, 10, and 100 h, the UTS values of the semi-solid thixoformed experimental alloys were 181, 122, and 110 MPa, respectively. The UTS values of the semi-solid thixoformed alloys were nearly two-fold higher than those of some of the heat-resistant aluminum alloys for commercial applications. The UTS of semi-solid thixoformed experimental alloys after thermal exposure at 300 °C for 100 h were increased by 37.5% and 31% as compared to the gravity die cast and squeeze cast alloys, respectively.

3.5 Fractured surfaces

Figure 13 illustrates the fractured surfaces of the experimental alloys after thermal exposure at 300 °C. All the fractured surfaces displayed the characteristics of a ductile fracture after elevated temperature thermal exposure. These characteristics increased with the rise in thermal exposure time. As shown in Figs. 13(a, b), several pores were found on the fractured surfaces of the gravity die cast alloy, which led to low elongation. Some small and deep dimples were observed on the fractured surfaces of squeeze cast alloys (Figs. 13(c, d)). The fractured surfaces of squeeze cast alloys displayed more ductile fracture features as compared to the gravity die cast alloys. The improvement of elongation in squeeze cast alloys can be attributed to the refinement of microstructure and decrease in

Table 2 Mechanical properties of Al−Si−Cu−Mn−Fe alloys and previously reported alloys after elevated temperature thermal exposure

Alloy (Condition)	Temperature/°C	UTS after thermal exposure/MPa			Source
		0.5 h	10 h	100 h	
GC (T6)	300	150	84	80	This work
SC (T6)	300	168	94	84	This work
SF (T6)	300	181	122	110	This work
2024 (T6)	315	110	85	69	[26]
6061 (T6)	315	85	62	41	[26]
7075 (T6)	315	70	62	59	[26]
356.0 (T6)	315	52	45	38	[26]
319.0 (T6)	315	90	75	66	[26]
Al−Si−Cu−Fe−Mn (T6)	300	144	−	−	[5]
Al−12Si−4Cu−2Ni−0.8Mg (T6)	300	109.5	−	−	[27]
Al−12Si−4Cu−2Ni−0.8Mg (T6)	300	140	−	−	[28]
Al−13.00Si−4Cu−0.92Mg−1.90Ni−0.16V (T6)	300	93	−	−	[29]
Al−13.72Si−2Cu−1.08Mg−2.36Ni−0.20V (T6)	300	94	−	−	[29]
Al−13.0Si−3.3Cu−1.3Mg−1.6Zn (T5)	315	132−145	−	−	[30]

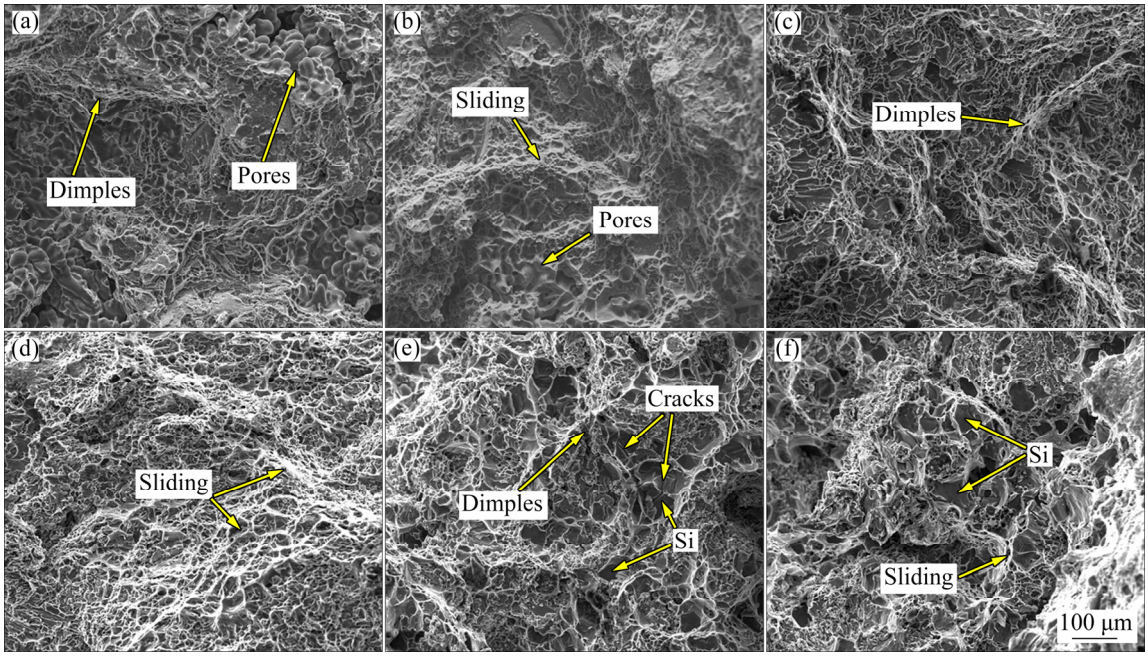

Fig. 13 Fractured surfaces of experimental alloys after thermal exposure at 300 °C: (a) Gravity die cast, 0.5 h; (b) Gravity die cast, 100 h; (c) Squeeze cast, 0.5 h; (d) Squeeze cast, 100 h; (e) Semi-solid thixoformed, 0.5 h; (f) Semi-solid thixoformed, 100 h

porosities and needle-like iron-rich intermetallics. Some block-shaped Si particles and cracks were found on the fractured surfaces of semi-solid thixoformed alloys. These results implied that the semi-solid thixoformed alloys demonstrated worse ductile failure features as compared to the squeeze cast alloys (Figs. 13(e, f)).

Figure 14 displays the morphologies of intermetallics and pores on or beneath the fractured surfaces of the experimental alloys in the longitudinal direction after thermal exposure at 300 °C. On the fractured surface of gravity die cast

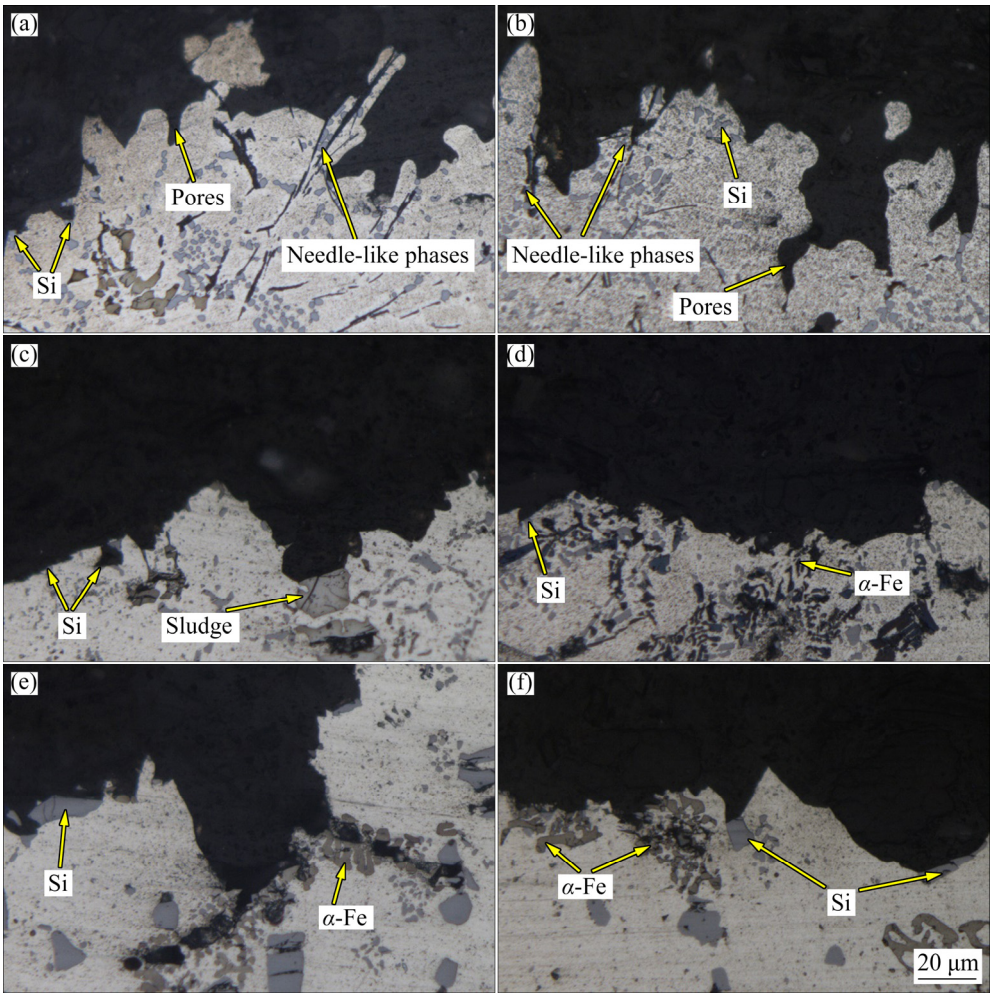

Fig. 14 Morphologies of intermetallics and pores on or beneath fractured surfaces of experimental alloys in longitudinal direction after exposure at 300 °C: (a) Gravity die cast, 0.5 h; (b) Gravity die cast, 100 h; (c) Squeeze cast, 0.5 h; (d) Squeeze cast, 100 h; (e) Semi-solid thixoformed, 0.5 h; (f) Semi-solid thixoformed, 100 h

alloys, large number of pores, eutectic Si particles, and needle-like intermetallics phases were observed on or beneath the fractured surface. These brittle intermetallics and pores in the gravity die cast alloys resulted in crack formation and propagation, which finally led to fracture failure (Figs. 14(a, b)). Numerous eutectic Si particles and iron-rich intermetallics (sludge or α-Fe) were observed on the fractured surface of squeeze cast alloys. The morphology of fractured surface in squeeze cast alloys suggested that the eutectic Si particles, sludge, or α-Fe were the main sources of cracks, which led to the fracture failure of squeeze cast alloys (Figs. 14(c, d)). As shown in Figs. 14(e, f), multiple coarse Si particles and α-Fe can be observed on or beneath the fractured surface of the semi-solid thixoformed alloys, which indicated that the coarse Si particles and α-Fe formed a weak location that resulted in the formation and propagation of cracks during tensile loading.

4 Discussion

4.1 Deterioration of elevated temperature tensile properties of squeeze cast alloys after long thermal exposure

As shown in Fig. 12, the tensile properties of squeeze cast alloys at elevated temperatures were higher than those of gravity die cast alloys after thermal exposure for 0.5 h, which then decreased to almost the same value as the thermal exposure time increased to 100 h. As per Fig. 7, the grain size of the squeeze cast alloy (118 μm) was significantly lower than that of the gravity die cast alloy (437 μm). In general, it is not suitable to develop the heat-resistant aluminum alloys by using refined

grain strengthening, as grain boundary movement or sliding often occurs at long elevated temperature thermal exposure. This phenomenon has been reported by LI et al [31]. They found that the grain refinement was beneficial to the improvement of room temperature tensile properties of Al−Si−Cu−Ni−Mg piston alloys. Also, the group observed that the tensile properties at 350 °C decreased, which was attributed to the grain refinement of grain size and non-uniform distribution of the heat resistant secondary intermetallic compound. Besides, QIAN [32] concluded that the squeeze casting is harmful to the elevated temperature tensile properties of Al−Si−Cu−Ni−Mg piston alloy, which was attributed to the increased precipitation of thermolabile Mg_2Si phases and refinement of grain size. In the current study, the decreased improvement of high temperature strength in squeeze cast alloys can be attributed to the grain boundary softening or sliding as a result of grain refinement, as well as the decrease in θ' phases during long thermal exposure compared with the gravity die cast alloys. As shown in Fig. 10, the amount of θ' phases in squeeze cast samples was more than that in the gravity die cast samples after thermal exposure for 0.5 h. However, amount of θ' phases in squeeze cast samples was nearly the same as that in the gravity die cast samples after thermal exposure for 100 h, indicating that the θ' phases were heat labile after long thermal exposure at 300 °C. DAR and LIAO [33] concluded that the θ' phases were heat labile in Al−Cu alloys when the thermal exposure temperature was above 300 °C. Consequently, the deterioration of elevated temperature tensile properties of the squeeze cast alloys after long thermal exposure can be attributed to the grain boundary softening or sliding and the decrease in θ' phases during long thermal exposure.

4.2 Enhanced elevated temperature tensile properties of semi-solid thixoformed alloys after long thermal exposure

The elevated temperature tensile properties of semi-solid thixoformed alloys demonstrate higher values as compared to the gravity die cast and squeeze cast alloys. As is well known, prevention of dislocation movement in α(Al) and grain boundary sliding is an efficient method to improve the elevated temperature tensile properties of heat-resistant Al alloys. The highly enhanced elevated temperature tensile properties of the experimental alloys fabricated via semi-solid thixoforming can be attributed to the combined reinforcement of precipitation strengthening and grain boundary strengthening owing to thermally stable intermetallic phases.

4.2.1 Grain boundary strengthening

In general, at elevated temperatures, the grain boundary softens, causing a decreased strength of heat-resistant aluminum alloys. Therefore, the formation of heat-resistant intermetallics around the grain boundary prevents grain boundary sliding, which amplifies the high temperature strength of heat-resistant aluminum alloys. As shown in Fig. 6, the morphologies of Fe-rich intermetallics and Si particles were not affected after thermal exposure at 300 °C for 100 h. After semi-solid isothermal treatment and semi-solid thixoforming, the eutectic Si particles again precipitated around the grain boundary, forming a chain-like distribution. These heat-resistant Fe-rich intermetallics and eutectic Si particles, which exhibit a chain-like distribution, can prevent grain boundary sliding in the Al−Si piston alloys during tensile loading at high temperatures. As has been reported earlier, the shape of heat-resistant secondary intermetallics phases also plays a great role in the elevated temperature tensile properties. YANG et al [34] noted that the grain boundary is the weak phase during long time thermal exposure. Compared to the coarse secondary intermetallics, the chain-type heat-resistant secondary intermetallics phases precipitated around the grain boundary can prevent the grain boundary sliding more effectively during thermal exposure. Figure 15 displays a TEM image

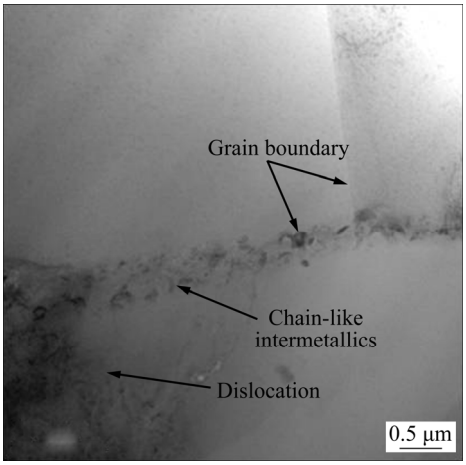

Fig. 15 TEM image showing dislocation prevention from intermetallic precipitates with chain-like distribution

where dislocation prevention from intermetallics with chain-like distribution can be observed, further validating the above results.

4.2.2 Precipitation strengthening

The formation of thermally stable intermetallic particles in the aluminum matrix prevents the dislocation movement, and it is known to amplify the high temperature strength of heat-resistant Al alloys [35]. The TEM images in Fig. 16 show the interaction between the precipitates and dislocations in the semi-solid thixoformed alloys. These results indicate that the *T* phases and *α*-Fe dispersoids can efficiently prevent dislocation motion and consume strain energy during tensile deformation, even after thermal exposure for 100 h. Multiple researchers have reported that *T* phases and *α*-Fe dispersoids in the Al−Cu and Al−Si alloys are thermally stable intermetallics, which favor the improvement of elevated temperature tensile properties [23,24]. In the precipitation-strengthened materials, high temperature strength can be explained in terms of Orowan bypass mechanism [36−38]. Therefore, the resultant high strength at high temperatures can be partially attributed to the precipitation strengthening of fine *T* phases and *α*-Fe particles.

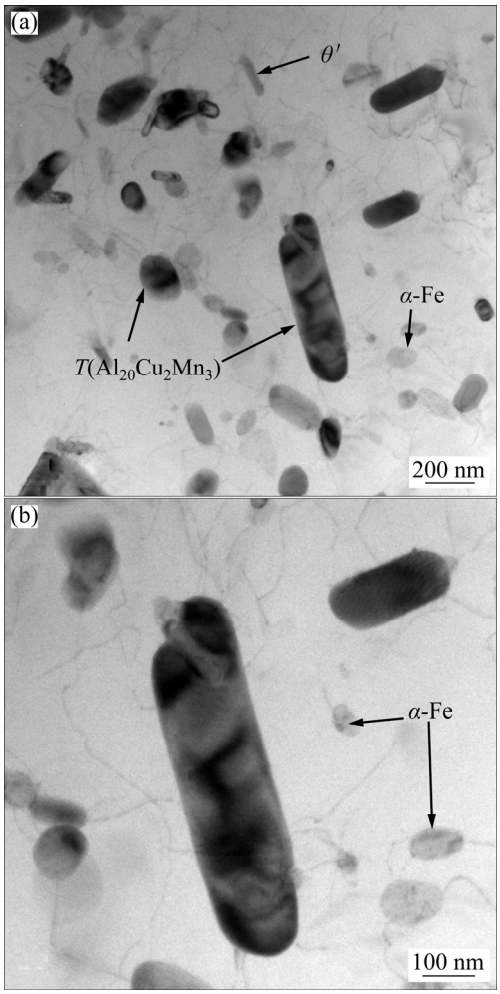

Fig. 16 TEM images revealing interactions between precipitates and dislocations in semi-solid thixoformed alloys

Suitable grain size and decrease in needle-like phases and pores in the semi-solid thixoformed alloys were also beneficial to the improvement of elevated temperature tensile properties after long thermal exposure. The decrease in elevated temperature tensile properties of the squeeze cast alloys after long thermal exposure further proves the importance of suitable grain size.

Herein, the combined reinforcement of precipitation strengthening and grain boundary strengthening due to thermally stable intermetallic phases as well as the suitable grain size was achieved by employing the semi-solid thixoforming method. The treatment led to highly enhanced elevated temperature tensile properties in the experimental alloys, especially, after long thermal exposure. This study is beneficial to the application of semi-solid aluminum alloys as light, heat-resistant, structural components in the military and marine industries. However, some pores could also be found in the semi-solid thixoformed samples, which indicates that the applied pressure is still inadequate. A higher applied pressure would be explored in our future work. As shown in Fig. 6, a few coarse Si particles were also found in the semi-solid thixoformed samples, which can be attributed to the growth of Si particles during semi-solid isothermal treatment for a long duration. Hence, the rapid heating technology and fast spheroidization treatment of *α*(Al) would be studied in our further work, such as induction heating, ultrasonic treatment, etc.

5 Conclusions

(1) The elevated temperature tensile properties of squeeze cast alloys demonstrated higher values than the gravity die cast alloys after thermal exposure for 0.5 h, which were then decreased to almost same values when the thermal exposure time was increased to 100 h. This result was attributed to the grain boundary softening or sliding and

decrease in θ' phases during long thermal exposure, implying that the squeeze cast technology is unsuitable for the development of heat-resistant aluminum alloys.

(2) The elevated temperature tensile properties of semi-solid thixoformed alloys demonstrated significantly higher values than those of the gravity die cast and squeeze cast alloys. The highly enhanced elevated temperature tensile properties after thermal exposure of experimental alloys formed by semi-solid thixoforming could be attributed to the combined reinforcement of precipitation strengthening (due to thermally stable mico-sized T ($Al_{20}Cu_2Mn_3$) and nano-sized α-Fe precipitated particles) and grain boundary strengthening (due to thermally stable chain-like Fe-rich intermetallics and eutectic Si particles). Suitable grain size and reduction in needle-like phases and pores in the semi-solid thixoforming alloys were also beneficial to the improvement of elevated temperature tensile properties after long thermal exposure.

(3) The UTS values of semi-solid thixo-formed alloys after thermal exposure at 300 °C for 0.5, 10, and 100 h were 181, 122, and 110 MPa, respectively. The UTS of semi-solid thixoformed alloys was nearly two-fold higher than those of the heat-resistant aluminum alloys for commercial applications. The UTS of semi-solid thixoformed experimental alloys at 300 °C after thermal exposure for 100 h increased by 37.5% and 31% as compared to the gravity die cast and squeeze cast alloys, respectively.

(4) The semi-solid thixoforming technique is an efficient method for the development of novel heat-resistant aluminum alloys by the combined reinforcement of precipitation strengthening and grain boundary strengthening due to thermally stable intermetallic phases, as well as the suitably adjusted grain size.

Acknowledgments

This work was financially supported by the National Natural Science Foundation of China (Nos. 51704084, 52074131), the Science and Technology Plan of Guizhou Province, China (Nos. ZK2021(267), ZK2021(067)), and the Cultivation Project of Guizhou University, China (No. 2019(23)).

References

[1] ZHANG Jia-ying, ZUO Li-jie, FENG Jian, et al. Effect of thermal exposure on microstructure and mechanical properties of Al−Si−Cu−Ni−Mg alloy produced by different casting technologies [J]. Transactions of Nonferrous Metals Society of China, 2020, 30(7): 1717−1730.

[2] DING Jian, ZHANG Pan, LI Xing-wen, WANG Li-sheng, LIAO Wen-zhe, HUANG Li-xin. Microstructure and thermal stability evolution behavior of Sc-containing A356. 2: Aluminum alloy under cyclic thermal exposure conditions [J]. Materials Science and Engineering A, 2018, 723: 165−173.

[3] TZENG Y C, CHENGN V S, NIEH J K. Microstructure and thermal stability of A357 alloy with and without the addition of Zr [J]. Journal of Materials Engineering and Performance, 2017, 26(11): 5511−5518.

[4] ABDELAZIZ M H, DOTY H W, VALTIERRA S, SAMUEL F H. Static versus dynamic thermal exposure of transition elements-containing Al−Si−Cu−Mg cast alloy [J]. Materials Science and Engineering A, 2019, 739: 499−512.

[5] WANG E R, HUI X D, CHEN G L. Eutectic Al−Si−Cu−Fe−Mn alloys with enhanced mechanical properties at room and elevated temperature [J]. Materials & Design, 2011, 32(8−9): 4333−4340.

[6] LIN Bo, LI Hao-yu, XU Rui, ZHAO Yu-liang. Thermal exposure of Al−Si−Cu−Mn−Fe alloys and its contribution to high temperature mechanical properties [J]. Journal of Materials Research and Technology, 2020, 9(2): 1856−1865.

[7] FLEMINGS M C, RIEK R G, YOUNG K P. Rheocasting [J]. Materials Science and Engineering A, 1976, 25: 103−117.

[8] RAJU K, KRISHNA N G, RAO L S. Microstructural features and wear characteristics of semi-solid processed A356 aluminum alloy [J]. Journal of Material Science and Technology Research, 2018, 5: 11−15.

[9] ZHANG Hong-tao, FAN Ling-ling, ZHOU Ming-yang, ZHANG Yu-wen-xi, LU Tian-hui, QUAN Gao-feng. Effects of semi-solid treatment by electro-magnetic induction on micro-structure evolution and mechanical properties of the Mg−2.4Y−4Nd−0.5Zr−1Ni alloys [J]. Materials Research Express, 2020, 7(5): 056506.

[10] KANG B K, SOHN I. Effects of Si content and forging pressure on the microstructural and mechanical characteristics in semi-solid forging of Al−Si−Mg alloys [J]. Metallurgical and Materials Transactions A, 2019, 50(7): 3213−3222.

[11] QI Ming-fan, KANG Yong-lin, LI Jing-yuan, SHANG Bei-yan. Improvement in mechanical, thermal conductivity and corrosion performances of a new high-thermally conductive Al−Si−Fe alloy through a novel R-HPDC process [J]. Journal of Materials Processing Technology, 2020, 279: 116586.

[12] KUMAR S D, MANDAL A, CHAKRABORTY M. On the age hardening behavior of thixoformed A356−5TiB_2 in-situ composite [J]. Material Science and Engineering A, 2015,

636(11): 254−262.

[13] KUMAR S D, MANDAL A, CHAKRABORTY M. Effect of thixoforming on the microstructure and tensile properties of A356 alloy and A356−5TiB_2 in-situ composite [J]. Transactions of Indian Institute of Metals, 2015, 68(2): 123−130.

[14] SALLEH M S, OMAR M Z, ALHAWARI K S, MOHAMMED M N, MADALI M A, MOHAMAD E. Microstructural evolution and mechanical properties of thixoformed A319 alloys containing variable amounts of magnesium [J]. Transactions of Nonferrous Metals Society of China, 2016, 26(8): 2029−2042.

[15] SALLEH M S, OMAR M Z, SYARIF J, AIHAWARI K S, MOHAMMED M N. Microstructure and mechanical properties of thixoformed A319 aluminium alloy [J]. Materials & Design, 2014, 64: 142−152.

[16] LIN Bo, XU Rui, LI Hao-yu, XIAO Hua-qiang, ZHANG Wei-wen, LI Shao-bo. Development of high Fe content squeeze cast 2A16 wrought Al alloys with enhanced mechanical properties at room and elevated temperatures [J]. Materials Characterization, 2018, 142: 389−397.

[17] XIAO Guan-fei, JIANG Ju-fu, LIU Ying-ze, WANG Ying, GUO Bao-yong. Recrystallization and microstructure evolution of hot extruded 7075 aluminum alloy during semi-solid isothermal treatment [J]. Materials Characterization, 2019, 156: 109874.

[18] JIANG Ju-fu, LIU Ying-ze, XIAO Guan-fei, WANG Ying, XIAO Xin-quan. Effects of plastic deformation of solid phase on mechanical properties and microstructure of wrought 5A06 aluminum alloy in directly semisolid thixoforging [J]. Journal of Alloys and Compounds, 2020, 831: 154748.

[19] LIU D, ATKINSON H V, JONES H. Thermodynamic prediction of thixoformability in alloys based on the Al−Si−Cu and Al–Si–Cu–Mg systems [J]. Acta Materialia, 2005, 53(14): 3807−3819.

[20] BIROL Y. A357 thixoforming feedstock produced by cooling slope casting [J]. Journal of Materials Processing Technology, 2007, 186(1−3): 94−101.

[21] HWANG J Y, DOTY H W, KAUFMAN M J. The effects of Mn additions on the microstructure and mechanical properties of Al−Si−Cu casting alloys [J]. Materials Science and Engineering A, 2008, 488(1−2): 496−504.

[22] SHABESTARI S G. The effect of iron and manganese on the formation of intermetallic compounds in aluminum–silicon alloys [J]. Materials Science and Engineering A, 2004, 383(2): 289−298.

[23] LIAO Heng-cheng, TANG Yun-yi, SUO Xiao-jing, LI Guang-jin, HU Yi-yun. Dispersoid particles precipitated during the solutionizing course of Al−12wt.%Si−4wt.%Cu−1.2wt.%Mn alloy and their influence on high temperature strength [J]. Materials Science and Engineering A, 2017, 699: 201−209.

[24] LIU K, CHEN X G. Improvement in elevated-temperature properties of Al−13%Si piston alloys by dispersoid strengthening via Mn addition [J]. Journal of Materials Research, 2018, 33(20): 3430−3438.

[25] RAKHMONOV J, LIU K, LEI P, BRETON F, CHEN X G. Enhanced mechanical properties of high-temperature-resistant Al−Cu cast alloy by microalloying with Mg [J]. Journal of Alloys and Compounds, 2020, 827: 154305.

[26] KAUFMAN J G. Properties of aluminum alloys: Tensile, creep, and fatigue data at high and low temperatures [M]. New York: ASM international, 1999.

[27] LIAN Han, SUI Yu-dong, WANG Qu-dong, WANG Kui, JIANG Ye-hua. Effects of Nd on microstructure and mechanical properties of cast Al−Si−Cu−Ni−Mg piston alloys [J]. Journal of Alloys and Compounds, 2017, 695: 1566−1572.

[28] SUI Yu-dong, JI De-peng, LIAN Han, WANG Qu-dong. Characterization of the aging precipitates of Al−12Si−4Cu−2Ni−0.8Mg−0.2Gd piston alloy [J]. JOM, 2019, 71(1): 366−372.

[29] AIKAWA T, ISHIKAWA A, HARA S. Aluminum alloy for internal-combustion piston and aluminum alloy piston: US patent, 5996471 [P]. 1999−12−7.

[30] TAKASAKI N, YOSHIMURA Y. Heat resistant Al die cast material: US patent, 6706242 [P]. 2004−3−16.

[31] LI Yun-guo. The study of elevated-temperature strengthening phase of Al−Si−Cu−Ni−Mg piston alloys [D]. Ji'nan: Shandong University, 2011. (in Chinese)

[32] QIAN Zhao. Study on high strength heat-resistant Al−Si piston alloys [D]. Jinan: Shandong University, 2009. (in Chinese)

[33] DAR S M, LIAO H C. Creep behavior of heat resistant Al–Cu–Mn alloys strengthened by fine (θ') and coarse ($Al_{20}Cu_2Mn_3$) second phase particles [J]. Materials Science and Engineering A, 2019, 763: 138062−138075.

[34] YANG Yang, LI Yun-guo, WU Wu-ying, ZHAO De-gang, LIU Xiang-fa. Effect of existing form of alloying elements on the microhardness of Al–Si–Cu–Ni–Mg piston alloy [J]. Materials Science and Engineering A, 2011, 528(18): 5723−5728.

[35] AMMAR H R, SAMUEL A M, SAMUEL F H. Aging behavior of 359-type Al−9%Si−0.5%Mg casting alloys [J]. Journal of Materials Science, 2012, 47(3): 1331−1338.

[36] JIAN Q, ZHANG Z, CHEN X G. Mechanical properties and strengthening mechanisms of Al−15%B_4C composites with Sc and Zr at elevated temperatures [J]. Metallurgical and Materials Transactions A, 2016, 47(9): 4694−4708.

[37] FULLER C B, SEIDMAN D N, DUNAND D C. Mechanical properties of Al (Sc, Zr) alloys at ambient and elevated temperatures [J]. Acta Materialia, 2003, 51: 4803−4814.

[38] LI Y J, MUGGERUD A M F, OLSEN A, FURU T. Precipitation of partially coherent α-Al(Mn,Fe)Si dispersoids and their strengthening effect in AA3003 alloy [J]. Acta Materialia, 2012, 60: 1004−1014.

半固态触变成形 Al−Si−Cu−Mn−Fe 合金的显微组织和高温拉伸力学性能

林 波[1]，范 滔[1]，李浩宇[1]，赵愈亮[2]，张卫文[3]，刘 坤[4]

1. 贵州大学 机械工程学院，贵阳 550025；
2. 东莞理工学院 机械工程学院，东莞 523808;
3. 华南理工大学 机械与汽车工程学院，广州 510640；
4. Department of Applied Science, University of Quebec at Chicoutimi, Quebec, Canada

摘 要：对比分析重力铸造、挤压铸造、半固态触变成形制备的 Al−Si−Cu−Mn−Fe 合金在 300 °C 热暴露下的组织演变和高温拉伸力学性能。结果表明：相比重力铸造和挤压铸造合金，半固态触变成形 Al−Si−Cu−Mn−Fe 合金具有更优异的高温力学性能，尤其是当热暴露时间为 100 h 时。半固态触变成形 Al−Si−Cu−Mn−Fe 合金在 300 °C 热暴露时间为 0.5、10 和 100 h 时的高温极限抗拉强度分别为 181、122 和 110 MPa, 高于大部分商用耐热铝合金。半固态触变成形 Al−Si−Cu−Mn−Fe 合金获得高强热暴露力学性能的主要原因是耐热相导致的晶界和晶内弥散协同强化以及合适的晶粒尺寸。

关键词：铝硅合金；富铁金属间化合物；半固态触变成形；显微组织；拉伸性能；热暴露

(Edited by Wei-ping CHEN)